

Learning a Compressive Sensing Matrix with Structural Constraints via Maximum Mean Discrepancy Optimization

Michael Koller and Wolfgang Utschick

Abstract—We introduce a learning-based algorithm to obtain a measurement matrix for compressive sensing related recovery problems. The focus lies on matrices with a constant modulus constraint which typically represent a network of analog phase shifters in hybrid precoding/combining architectures. We interpret a matrix with restricted isometry property as a mapping of points from a high- to a low-dimensional hypersphere. We argue that points on the low-dimensional hypersphere, namely, in the range of the matrix, should be uniformly distributed to increase robustness against measurement noise. This notion is formalized in an optimization problem which uses one of the maximum mean discrepancy metrics in the objective function. Recent success of such metrics in neural network related topics motivate a solution of the problem based on machine learning. Numerical experiments show better performance than random measurement matrices that are generally employed in compressive sensing contexts. Further, we adapt a method from the literature to the constant modulus constraint. This method can also compete with random matrices and it is shown to harmonize well with the proposed learning-based approach if it is used as an initialization. Lastly, we describe how other structural matrix constraints, e.g., a Toeplitz constraint, can be taken into account, too.

Index Terms—compressive sensing, machine learning, maximum mean discrepancy, restricted isometry property, sparse channel estimation

I. INTRODUCTION

IN the context of possible technologies for up-and-coming cellular systems, millimeter wave systems with a high number of antennas have been proposed [1]–[5]. One way of controlling hardware costs and power consumption is to connect the antennas to a smaller number of receiver chains, which is done via an analog mixing network [6]–[10]. For data transmission, digital precoding is combined with configuring the analog mixing network (analog precoding).

In order to design both of these precoding stages (hybrid precoding), state information of the high-dimensional channel is necessary. However, the presence of an analog mixing network makes channel estimation challenging because the observation vector has a smaller dimension (number of receiver chains) than the channel vector (number of antennas) which is to be estimated. To facilitate channel estimation in this situation, channel models can play an important role. In particular, sparsity-related structural knowledge about channels in millimeter wave systems has been exploited, e.g., [11]–[13].

This naturally leads to the application of compressive sensing (CS) theory in channel estimation contexts where the analog mixing network then plays the role of the measurement or sensing matrix. Among the best known conditions suitable measurement matrices should fulfill is the restricted isometry property (RIP) (e.g., [14]). Since deterministic constructions of measurement matrices with RIP are not known, the CS theory uses random matrices which enjoy favorable properties with high probability [14].

One challenge with analog mixing networks is that they cannot realize any random matrix. Rather, the hardware is constrained to provide matrix entries with constant modulus, i.e., only the phase of the entries can be adapted. Additionally, it can be argued that such phase shifter matrices might only be able to provide a finite number of different phases (quantized phases, e.g., [15]), thus making the realization of random matrices that are dictated by the CS theory more difficult.

In this paper, we propose a learning-based approach to find a deterministic measurement matrix for channel estimation. The main idea is to interpret a matrix with RIP as a matrix which (approximately) maps points from a high-dimensional hypersphere to a low-dimensional hypersphere. Moreover, we suggest to choose the matrix such that in addition the points in its range (on the low-dimensional hypersphere) are uniformly distributed in order to combat the influence of measurement noise, which typically exists in communications systems.

We use one of the maximum mean discrepancy (MMD) metrics [16] as learning cost function to formalize the idea. MMD-based cost functions have had considerable success in machine learning, e.g., for generative networks [17]–[19]. In numerical experiments, the matrix obtained from the proposed algorithm is shown to compete with or outperform the approach based on random matrices. It may be argued that such a deterministic matrix might be easier to realize via an analog mixing network than random matrices.

Furthermore, we adapt an algorithm from [20] to the phase shifter constant modulus constraint and demonstrate its good performance in numerical experiments as well. In addition, this algorithm is shown to harmonize well with the learning-based approach of the current paper by providing an initialization of the learning algorithm.

The rest of this paper is organized as follows. Section II introduces the signal model as well as CS background. The main idea including a brief introduction to MMD is outlined in Section III. An overview of prior work and the modification of [20] is presented in Section IV. Finally, numerical exper-

The authors are with Professur für Methoden der Signalverarbeitung, Technische Universität München, 80333 München, Germany, e-mail: michael.koller@tum.de, utschick@tum.de

iments are conducted in Section V which is followed by a conclusion.

Notation: We write $\exp(\mathbf{X})$, $\sin(\mathbf{X})$, $\cos(\mathbf{X})$ for element-wise application of the exponential, sine, and cosine functions to a matrix \mathbf{X} . Transpose and conjugate transpose of vectors $\mathbf{x} \in \mathbb{C}^n$ are denoted as \mathbf{x}^T and \mathbf{x}^H , respectively. We use $\langle \cdot, \cdot \rangle$ for the Euclidean inner product and $\|\cdot\|$ for its corresponding norm. Lastly, the complex normal probability distribution with mean $\mathbf{0}_m \in \mathbb{C}^m$ and noise covariance $\sigma^2 \mathbf{I}_m \in \mathbb{C}^{m \times m}$ is written as $\mathcal{CN}(\mathbf{0}_m, \sigma^2 \mathbf{I}_m)$.

II. PRELIMINARIES

In what follows, the signal model is

$$\mathbf{y} = \mathbf{A}\mathbf{h} + \mathbf{n} \quad (1)$$

where $\mathbf{A} \in \mathbb{C}^{m \times n}$ is called measurement matrix (with $m < n$), $\mathbf{h} \in \mathbb{C}^n$ is called channel, $\mathbf{y} \in \mathbb{C}^m$ is a measurement or an observation, and $\mathbf{n} \sim \mathcal{CN}(\mathbf{0}_m, \sigma^2 \mathbf{I}_m)$ corresponds to measurement noise. The matrix \mathbf{A} represents an analog mixing network with phase shifters so that the matrix entries $[\mathbf{A}]_{k,l}$ have the form

$$[\mathbf{A}]_{k,l} = \frac{1}{\sqrt{m}} \exp(j \phi_{k,l}) \quad (2)$$

with a phase $\phi_{k,l} \in \mathbb{R}$. All entries have a constant modulus constraint, $|[\mathbf{A}]_{k,l}| = 1/\sqrt{m}$, which is why we refer to such a matrix as constant modulus matrix.

This paper provides two methods to determine a constant modulus measurement matrix \mathbf{A} for recovering \mathbf{h} from (1). The main contribution is a novel learning-based algorithm. Additionally, we adapt a method from the literature to the constant modulus constraint. This method computes a different matrix \mathbf{A} for every signal-to-noise ratio (SNR), whereas the learning-based algorithm yields a single matrix which can be employed for all SNRs. We define the SNR as

$$\text{SNR} = \frac{\|\mathbf{A}\mathbf{h}\|^2}{\mathbb{E}[\|\mathbf{n}\|^2]} = \frac{\|\mathbf{A}\mathbf{h}\|^2}{m\sigma^2}, \quad (3)$$

where the noise variance σ^2 is adjusted for every pair (\mathbf{A}, \mathbf{h}) to achieve the desired SNR.

Since the goal is to estimate the n -dimensional channel from an m -dimensional observation with $m < n$, the inverse problem (1) generally has no unique solution. However, it is well known from CS theory that a unique solution can exist if additional structural information about the channels is available. One channel model that was studied in this context (see, e.g., [12], [13]) can be written as

$$\mathbf{h} = \sum_{k=1}^p s_k \mathbf{a}(\theta_k) \quad (4)$$

which corresponds to a sum of p paths which arrive from angles $\theta_k \in [0, 2\pi]$ with path gains $s_k \in \mathbb{C}$ at the base station. For a uniform linear array at the base station, the steering vector $\mathbf{a}(\theta_k) \in \mathbb{C}^n$ has the form

$$\mathbf{a}(\theta_k) = \frac{1}{\sqrt{n}} [\exp(j0 \cdot \theta_k) \quad \dots \quad \exp(j(n-1) \cdot \theta_k)]^T. \quad (5)$$

We briefly highlight relevant parts of CS theory in the next section where we then explain how CS is used with this channel model.

Algorithm 1 Orthogonal Matching Pursuit (OMP) [14]

Require: matrix \mathbf{C} , observation \mathbf{y} , sparsity p

- 1: $S^{(0)} \leftarrow \emptyset$, $\mathbf{s}^{(0)} \leftarrow \mathbf{0}$
 - 2: **for** $i = 1$ to p **do**
 - 3: $j^* \leftarrow \arg \max_{j \in \{1, \dots, n\}} \{[\mathbf{C}^H(\mathbf{y} - \mathbf{C}\mathbf{s}^{(i-1)})]_j\}$
 - 4: $S^{(i)} \leftarrow S^{(i-1)} \cup \{j^*\}$
 - 5: $\mathbf{s}^{(i)} \leftarrow \arg \min_{\tilde{\mathbf{s}}} \{\|\mathbf{y} - \mathbf{C}\tilde{\mathbf{s}}\|, \text{support}(\tilde{\mathbf{s}}) \subset S^{(i)}\}$
 - 6: **end for**
 - 7: **return** $\mathbf{s}^{(p)}$ (p -sparse vector)
-

A. Compressive Sensing

CS studies the inverse problem (1) for general (no constant modulus constraint) matrices $\mathbf{B} \in \mathbb{C}^{m \times n}$. In the case where $\mathbf{h} = \mathbf{s} \in \mathbb{C}^n$ is a p -sparse vector (p nonzero entries), it can be recovered if \mathbf{B} has a sufficient RIP [14]. A matrix $\mathbf{B} \in \mathbb{C}^{m \times n}$ is said to have the RIP if the restricted isometry constant $\delta \geq 0$ is small in

$$(1 - \delta)\|\mathbf{s}\|^2 \leq \|\mathbf{B}\mathbf{s}\|^2 \leq (1 + \delta)\|\mathbf{s}\|^2 \quad (6)$$

for all p -sparse vectors $\mathbf{s} \in \mathbb{C}^n$ [14].

More generally, it may be assumed that the signals of interest, \mathbf{h} , allow for a sparse representation $\mathbf{h} = \mathbf{\Psi}\mathbf{s}$ in some basis $\mathbf{\Psi} \in \mathbb{C}^{n \times n}$ such that the RIP condition is formulated where \mathbf{s} is replaced with $\mathbf{\Psi}\mathbf{s}$. Even more generally, \mathbf{h} may lie in an (infinite) union of subspaces or some abstract subset $\mathcal{H} \subset \mathbb{C}^n$ (see, e.g., [21]–[23]) and one defines a generalized notion of RIP as

$$(1 - \delta)\|\mathbf{h}\|^2 \leq \|\mathbf{B}\mathbf{h}\|^2 \leq (1 + \delta)\|\mathbf{h}\|^2 \quad (7)$$

for all $\mathbf{h} \in \mathcal{H}$.

One way of translating the model (4) into a CS setting is to introduce a so-called dictionary

$$\mathbf{\Psi}_L = [\mathbf{a}(\hat{\theta}_1) \quad \dots \quad \mathbf{a}(\hat{\theta}_L)] \in \mathbb{C}^{n \times L} \quad (8)$$

which collects L steering vectors corresponding to a grid of L equidistantly sampled angles $\hat{\theta}_\ell$ in $[0, 2\pi]$. Then, one approximates $\mathbf{h} \approx \mathbf{\Psi}_L \mathbf{s}$ with a p -sparse vector $\mathbf{s} \in \mathbb{C}^L$ which contains the path gains. Channel estimation can now be performed by writing

$$\tilde{\mathbf{y}} = (\mathbf{A}\mathbf{\Psi}_L)\mathbf{s} + \mathbf{n} \quad (9)$$

and by using for example orthogonal matching pursuit (OMP) [24]–[26] to recover an estimate $\hat{\mathbf{s}}$ of \mathbf{s} so that the channel is estimated as $\hat{\mathbf{h}} = \mathbf{\Psi}_L \hat{\mathbf{s}}$. OMP is described in Algorithm 1 and would be used with $\mathbf{C} = \mathbf{A}\mathbf{\Psi}_L$, see, e.g., [12]. Note that (9) is just an auxiliary approximation of (1) because $\mathbf{\Psi}_L \mathbf{s}$ is an approximation of \mathbf{h} . In particular, channels of the form (4) do not have an exact representation in terms of $\mathbf{\Psi}_L$ whenever $\theta_k \notin \{\hat{\theta}_1, \dots, \hat{\theta}_L\}$ for some $k = 1, \dots, p$.

To obtain a matrix with RIP, one usually resorts to drawing random matrices which can fulfill the property with high probability [14]. A typical example is a Gaussian random matrix $\mathbf{B} \in \mathbb{C}^{m \times n}$ where the entries are drawn independently with $[\mathbf{B}]_{k,l} \sim \mathcal{CN}(0, \frac{1}{\sqrt{m}})$. These, however, cannot be realized via an analog mixing network. More generally, sub-Gaussian random matrices have been shown to fulfill the

RIP [14]. Sub-Gaussian random variables include bounded random variables [14]. Thus, it makes sense to consider random constant modulus matrices \mathbf{A} which are randomly drawn with independent entries of the form

$$\frac{1}{\sqrt{m}} \exp(j\phi) \quad \text{with} \quad \phi \sim \mathcal{U}([0, 2\pi]) \quad (10)$$

where ϕ is uniformly distributed in the interval $[0, 2\pi]$.

III. LEARNING A MEASUREMENT MATRIX

To motivate the main idea of this paper, we first rewrite the RIP condition (7) in the form

$$(1 - \delta) \leq \left\| \mathbf{B} \frac{\mathbf{h}}{\|\mathbf{h}\|} \right\|^2 \leq (1 + \delta) \quad (11)$$

for all $\mathbf{h} \in \mathcal{H}$. Recovery algorithms need $\delta \geq 0$ to be small enough. In the best case, we have $\delta = 0$ and (11) reads

$$\left\| \mathbf{B} \frac{\mathbf{h}}{\|\mathbf{h}\|} \right\|^2 = 1. \quad (12)$$

Here, $\tilde{\mathbf{h}} := \frac{\mathbf{h}}{\|\mathbf{h}\|}$ is a vector on the (high-dimensional) hypersphere in \mathbb{C}^n and according to (12) the matrix \mathbf{B} has the property that the vector $\mathbf{B}\tilde{\mathbf{h}}$ lies on the (low-dimensional) hypersphere in \mathbb{C}^m . In the general case, in order for δ to be as small as possible, (11) requires the norm $\|\mathbf{B}\tilde{\mathbf{h}}\|$ to be as close to one as possible. In other words, we want to find a matrix which brings $\mathbf{B}\tilde{\mathbf{h}}$ as close to the hypersphere in \mathbb{C}^m as possible.

Let $\mathbf{h}, \mathbf{h}' \in \mathcal{H}$ be two different vectors and let $\mathbf{y} = \mathbf{B}\mathbf{h}$ and $\mathbf{y}' = \mathbf{B}\mathbf{h}'$ be the corresponding noiseless observations. The RIP formalizes the notion that the distance between \mathbf{y} and \mathbf{y}' should be proportional to the distance between \mathbf{h} and \mathbf{h}' such that two vectors \mathbf{h}, \mathbf{h}' which are far apart from each other do not lead to the same observation even if the observations are noisy. As a consequence, \mathbf{h} and \mathbf{h}' can still be uniquely recovered if the noise is small. In this sense, the RIP guarantees some robustness against measurement noise.

In the spirit of the above description, it seems sensible in general to try to find a matrix \mathbf{B} which places two different observations far apart from each other, so that even in the presence of noise, they are distinguishable. When we work with the normalized vectors $\tilde{\mathbf{h}}$, this means that we now have two goals: On the one hand, $\|\mathbf{B}\tilde{\mathbf{h}}\|$ should be close to one in order to achieve a RIP, on the other hand, two different $\mathbf{B}\tilde{\mathbf{h}}$ and $\mathbf{B}\tilde{\mathbf{h}}'$ should be far apart from each other. The latter goal can also be formulated as follows: We want to find a matrix \mathbf{B} which distributes $\mathbf{B}\tilde{\mathbf{h}}$ isotropically around the origin.

To cast this idea into an optimization problem, let \mathbf{u} be a random variable which is uniformly distributed on the hypersphere in \mathbb{C}^m . That is, we have $\|\mathbf{u}\| = 1$ and \mathbf{u} is isotropically distributed around the origin. Further, let all elements in \mathcal{H} be realizations of a random variable \mathbf{h} and consider again the normalized $\tilde{\mathbf{h}}$. Then, if d denotes a (for now generic) distance between the distributions of $\mathbf{B}\tilde{\mathbf{h}}$ and \mathbf{u} , the goal is to choose \mathbf{B} such that this distance is minimized. Together with the original

goal to find a suitable constant modulus matrix \mathbf{A} , we arrive at the abstract optimization problem:

$$\min_{\mathbf{A} \in \mathbb{C}^{m \times n}, \|\mathbf{A}\|_{k,l} = \frac{1}{\sqrt{m}}} d(\mathbf{A}\tilde{\mathbf{h}}, \mathbf{u}). \quad (13)$$

We make this notion more precise in Section III-B. To this end, Section III-A first reviews the concept of MMDs which can be used to define a distance between probability distributions.

The optimization problem (13) encodes three goals. In order for $\mathbf{A}\tilde{\mathbf{h}}$ to be uniformly distributed on the hypersphere, the norm $\|\mathbf{A}\tilde{\mathbf{h}}\|$ needs to be as close to one as possible since the norm of \mathbf{u} always equals one. This corresponds to finding a matrix which has the RIP with δ in (11) as small as possible. At the same time, $\mathbf{A}\tilde{\mathbf{h}}$ needs to be isotropically distributed around the origin because this is a property of \mathbf{u} . This corresponds to placing noiseless observations far apart from each other. Therefore, problem (13) simultaneously aims for a RIP condition as well as for robustness against noise. Finally, due to the constraints, we obtain a constant modulus matrix.

A. Maximum Mean Discrepancy (MMD)

To state problem (13) more precisely, a distance between the probability distributions of $\mathbf{A}\tilde{\mathbf{h}}$ and \mathbf{u} is necessary. Many distances, for example the Kullback-Leibler divergence, can only be evaluated if closed-form expressions of the distributions are available or if the distributions are estimated beforehand. In the general case, we have access to samples of the channel \mathbf{h} , which are, e.g., obtained from a simulation environment or a measurement campaign. Moreover, the distribution of \mathbf{h} , and thus in particular also of $\mathbf{A}\tilde{\mathbf{h}}$, is not known. It is therefore more convenient to work with a distance which can be evaluated based on samples from the involved distributions, i.e., samples of $\mathbf{A}\tilde{\mathbf{h}}$ and \mathbf{u} . In the following, we introduce one of the MMD distances which has this property.

Let (\mathcal{X}, d) be a metric space and let \mathbf{x} and \mathbf{y} be two random variables with respective probability measures p and q . MMD provides the possibility to define a metric on the space of probability measures on \mathcal{X} . For a given set \mathcal{F} of functions $f : \mathcal{X} \rightarrow \mathbb{R}$, MMD is defined as [16, Definition 2]

$$\text{MMD}_{\mathcal{F}}(p, q) = \sup_{f \in \mathcal{F}} (\mathbb{E}_{\mathbf{x} \sim p}[f(\mathbf{x})] - \mathbb{E}_{\mathbf{y} \sim q}[f(\mathbf{y})]). \quad (14)$$

Depending on how \mathcal{F} is chosen, MMD can be a metric and then we have $\text{MMD}_{\mathcal{F}}(p, q) = 0$ if and only if $p = q$, and $\text{MMD}_{\mathcal{F}}(p, q) > 0$ otherwise. An overview of suitable function sets \mathcal{F} can, e.g., be found in [27].

Even if MMD is a metric, the evaluation of (14), i.e., solving the optimization problem, might still be difficult. One particularly interesting set \mathcal{F} in this regard is the unit ball in a reproducing kernel Hilbert space (RKHS). A brief introduction into RKHS can be found in [16]. Every RKHS is a Hilbert space which is associated with a kernel $k : \mathcal{X} \times \mathcal{X} \rightarrow \mathbb{R}$. And, conversely, every kernel defines an associated RKHS. Intuitively speaking, a kernel k can represent all functions which are an element of the RKHS. For this reason, the optimization w.r.t. the whole set \mathcal{F} in (14) can be expressed by

means of the kernel only and the computation of the supremum is avoided.

Among the best known kernels is the Gaussian one:

$$k_\sigma : \mathbb{R}^{2m} \times \mathbb{R}^{2m} \rightarrow \mathbb{R}, (\mathbf{x}, \mathbf{y}) \mapsto k_\sigma(\mathbf{x}, \mathbf{y}) = e^{-\frac{1}{2\sigma^2} \|\mathbf{x} - \mathbf{y}\|^2} \quad (15)$$

with a parameter $\sigma > 0$. Using the Gaussian kernel, (14) can be expressed as [16, Lemma 6]

$$\text{MMD}_k^2(p, q) = \mathbb{E}_{\mathbf{x}, \mathbf{x}'}[k(\mathbf{x}, \mathbf{x}')] - 2 \mathbb{E}_{\mathbf{x}, \mathbf{y}}[k(\mathbf{x}, \mathbf{y})] + \mathbb{E}_{\mathbf{y}, \mathbf{y}'}[k(\mathbf{y}, \mathbf{y}')] \quad (16)$$

and it is a metric. Here, \mathbf{x} and \mathbf{x}' are independent random variables with distribution p , and \mathbf{y} and \mathbf{y}' are independent random variables with distribution q . The Gaussian kernel is a typical choice when MMD_k is used, as, e.g., [17], [19], [28] demonstrate. One reason is that the associated RKHS enjoys the property of being universal which makes (16) a metric [16, Theorem 5].

If only samples $\{\mathbf{x}_i\}_{i=1}^M$ and $\{\mathbf{y}_j\}_{j=1}^N$ of $\mathbf{x} \sim p$ and $\mathbf{y} \sim q$, respectively, are given, (16) allows for a biased estimate [16, Equation (5)]:

$$\begin{aligned} \text{MMD}_k^2(\{\mathbf{x}_i\}_{i=1}^M, \{\mathbf{y}_j\}_{j=1}^N) &= \sum_{i=1}^M \sum_{j=1}^M \frac{k(\mathbf{x}_i, \mathbf{x}_j)}{M^2} \\ &\quad - 2 \sum_{i=1}^M \sum_{j=1}^N \frac{k(\mathbf{x}_i, \mathbf{y}_j)}{MN} + \sum_{i=1}^N \sum_{j=1}^N \frac{k(\mathbf{y}_i, \mathbf{y}_j)}{N^2}. \end{aligned} \quad (17)$$

Throughout the paper, we employ this estimate (17) which converges in probability to (16) at a rate of $\mathcal{O}((M+N)^{-\frac{1}{2}})$, see [16, Theorem 7]. A detailed analysis of the metric can be found in [16].

Since the kernel (15) is differentiable, so is MMD_k . This, together with the fact that only samples from the involved distributions are required, makes (17) interesting for learning applications. For example, [17] uses MMD_k as neural network cost function in the context of data generation. There, a set of true images is given and the goal is to find a function which takes random noise as argument and yields artificial new images as function values. The function is chosen to be a neural network and the goal is to minimize MMD_k between its output and the true images, so that the neural network is able to generate photo-realistic images which resemble the true ones. The minimization problem is solved via stochastic gradient descent with impressive results.

B. Learning

With the help of MMD, we express (13) as a learning problem. To this end, we want to replace the notion of a generic distance d in (13) between $\mathbf{A}\tilde{\mathbf{h}}$ and \mathbf{u} with MMD_k .

For this purpose, we represent $\mathbf{A}\tilde{\mathbf{h}}$ and \mathbf{u} in terms of real quantities because it also simplifies the implementation. Let

$$\text{stk} : \mathbb{C}^m \rightarrow \mathbb{R}^{2m}, \mathbf{z} \mapsto \text{stk}(\mathbf{z}) = [\Re(\mathbf{z})^T, \Im(\mathbf{z})^T]^T \quad (18)$$

denote stacking real and imaginary parts of a complex vector \mathbf{z} into a real vector $\text{stk}(\mathbf{z})$. Further, let $\{\tilde{\mathbf{h}}_i\}_{i=1}^{T_{\text{tr}}}$ and $\{\mathbf{u}_i\}_{i=1}^{T_{\text{tr}}}$ be training samples. Here, $\{\tilde{\mathbf{h}}_i\}_{i=1}^{T_{\text{tr}}}$ is a sample of normalized

channel data points and $\{\mathbf{u}_i\}_{i=1}^{T_{\text{tr}}}$ a set of points drawn from a uniform distribution on the hypersphere in \mathbb{C}^m . The channel data points may either stem from a measurement campaign or may be artificially generated according to a channel model. A random vector \mathbf{u} with uniform distribution on the hypersphere in \mathbb{C}^m is obtained via normalization of an isotropic Gaussian random vector, e.g., $\mathbf{u} = \frac{\mathbf{v}}{\|\mathbf{v}\|}$ with $\mathbf{v} \sim \mathcal{CN}(\mathbf{0}_m, \mathbf{I}_m)$, which means that sampling is simple. We then express (13) as follows:

$$\min_{\substack{\mathbf{A} \in \mathbb{C}^{m \times n} \\ \|\mathbf{A}\|_{k,l} = \frac{1}{\sqrt{m}}}} \text{MMD}_k^2(\{\text{stk}(\mathbf{A}\tilde{\mathbf{h}}_i)\}_{i=1}^{T_{\text{tr}}}, \{\text{stk}(\mathbf{u}_i)\}_{i=1}^{T_{\text{tr}}}). \quad (19)$$

Next, we address the constant modulus constraint $\|\mathbf{A}\|_{k,l} = 1/\sqrt{m}$ and express the optimization problem in terms of real optimization variables instead of $\mathbf{A} \in \mathbb{C}^{m \times n}$. Note that since every entry of $\mathbf{A} \in \mathbb{C}^{m \times n}$ has to have the form $[\mathbf{A}]_{k,l} = \frac{1}{\sqrt{m}} \exp(j\phi_{k,l})$ with a phase $\phi_{k,l} \in \mathbb{R}$, the constant modulus matrix \mathbf{A} is completely parameterized by mn real parameters. We collect these parameters in a matrix $\Phi \in \mathbb{R}^{m \times n}$ such that we can write $\mathbf{A} = \frac{1}{\sqrt{m}} \exp(j\Phi)$ where the exponential function is meant to be applied element-wise and where the constraint $\|\mathbf{A}\|_{k,l} = \frac{1}{\sqrt{m}}$ is already incorporated. If also sin and cos are applied element-wise, we can write

$$\mathbf{A} = \Re(\mathbf{A}) + j\Im(\mathbf{A}) = \frac{1}{\sqrt{m}} \cos(\Phi) + j \frac{1}{\sqrt{m}} \sin(\Phi) \quad (20)$$

so that we get from $\mathbf{A}\tilde{\mathbf{h}} = (\Re(\mathbf{A}) + j\Im(\mathbf{A}))(\Re(\tilde{\mathbf{h}}) + j\Im(\tilde{\mathbf{h}}))$:

$$\text{stk}(\mathbf{A}\tilde{\mathbf{h}}) = \begin{bmatrix} \Re(\mathbf{A}\tilde{\mathbf{h}}) \\ \Im(\mathbf{A}\tilde{\mathbf{h}}) \end{bmatrix} = \begin{bmatrix} \frac{\cos(\Phi)}{\sqrt{m}} & -\frac{\sin(\Phi)}{\sqrt{m}} \\ \frac{\sin(\Phi)}{\sqrt{m}} & \frac{\cos(\Phi)}{\sqrt{m}} \end{bmatrix} \begin{bmatrix} \Re(\tilde{\mathbf{h}}) \\ \Im(\tilde{\mathbf{h}}) \end{bmatrix}. \quad (21)$$

Equation (21) reveals that $\text{stk}(\mathbf{A}\tilde{\mathbf{h}})$ only depends on $\mathbf{A} \in \mathbb{C}^{m \times n}$ via the real matrix $\Phi \in \mathbb{R}^{m \times n}$. Let us express this as $\text{stk}(\mathbf{A}\tilde{\mathbf{h}}) = \text{stk}(\mathbf{A}(\Phi)\tilde{\mathbf{h}})$ so that we can rewrite (19) as a real optimization problem:

$$\min_{\Phi \in \mathbb{R}^{m \times n}} \text{MMD}_k^2(\{\text{stk}(\mathbf{A}(\Phi)\tilde{\mathbf{h}}_i)\}_{i=1}^{T_{\text{tr}}}, \{\text{stk}(\mathbf{u}_i)\}_{i=1}^{T_{\text{tr}}}). \quad (22)$$

In the literature, such optimization problems are solved via stochastic gradient descent, e.g., [17], [19], [28], [29]. Since gradient descent can be employed and seems to yield good results, MMD-based problems are considered to be easy to optimize [29]. Accordingly, we also use stochastic gradient descent to solve problem (22). The details are summarized in Algorithm 2. General convergence guarantees are part of ongoing research. The standard procedure in machine learning is to employ some form of grid or random search over various hyperparameters of the stochastic gradient descent algorithm in combination with random initializations of the optimization parameters. A validation data set is then used to choose the best solution. Possible hyperparameter values for Algorithm 2 are described in Section V-B.

In every iteration of Algorithm 2, MMD_k^2 and its gradient need to be calculated. With backpropagation, evaluating the gradient has the same order of computation time as the forward pass [30]. To compute MMD_k^2 for a batch of T samples, the kernel is evaluated $\mathcal{O}(T^2)$ times, see (17), with vectors of dimension $2m$ (stacked real and imaginary parts).

Algorithm 2 Learning $\mathbf{A} = \mathbf{A}(\Phi)$

Require: training data $\{(\tilde{\mathbf{h}}_i, \mathbf{u}_i)\}_{i=1}^{T_{\text{tr}}}$

- 1: randomly initialize $\Phi \in [0, 2\pi]^{m \times n}$
- 2: **while** termination criterion not met **do**
- 3: draw a batch of T samples uniformly from the training data: $\{(\tilde{\mathbf{h}}_t, \mathbf{u}_t)\}_{t=1}^T \subset \{(\tilde{\mathbf{h}}_i, \mathbf{u}_i)\}_{i=1}^{T_{\text{tr}}}$
- 4: compute the stochastic gradient

$$\mathbf{g}_\Phi = \frac{\partial}{\partial \Phi} \text{MMD}_k^2(\{\text{stk}(\mathbf{A}(\Phi)\tilde{\mathbf{h}}_t)\}_{t=1}^T, \{\text{stk}(\mathbf{u}_t)\}_{t=1}^T)$$
- 5: update Φ with a gradient algorithm using \mathbf{g}_Φ
- 6: **end while**

Since $\text{stk}(\mathbf{A}\tilde{\mathbf{h}})$ can be computed in $\mathcal{O}(mn)$ time, the overall computation time is $\mathcal{O}(mnT + 2mT^2)$. As an alternative, [16, Lemma 14] could be used, where a linear (in T) version of MMD is introduced such that the computation time would be $\mathcal{O}(mnT)$.

IV. RELATED WORK

This section reviews prior work related to learning a measurement matrix and describes a modification of one of the presented methods which allows us to employ it in the context of the signal model described in Section II.

A. Prior Work

The authors of [31] consider the real-valued signal model $\mathbf{y} = \mathbf{B}\mathbf{h} + \mathbf{n}$ where $\mathbf{B} \in \mathbb{R}^{m \times n}$ is a general real matrix. Their *Uncertain Component Analysis* determines the matrix as

$$\mathbf{B} = \arg \max_{\tilde{\mathbf{B}} \in \mathbb{R}^{m \times n}, \tilde{\mathbf{B}}\tilde{\mathbf{B}}^T = \mathbf{I}} \prod_i \Pr(\mathbf{h}_i | \mathbf{y}_i; \tilde{\mathbf{B}}) \quad (23)$$

with given data points \mathbf{h}_i and $\mathbf{y}_i = \tilde{\mathbf{B}}\mathbf{h}_i$ and where $\Pr(\mathbf{h}_i | \mathbf{y}_i; \tilde{\mathbf{B}})$ is the posterior probability of the data. An algorithmic solution based on two fixed-point equations is proposed.

In [32], the signal model is $\mathbf{y} = \mathbf{B}\Psi\mathbf{s}$ with $\mathbf{B} \in \mathbb{R}^{m \times n}$ and $\Psi \in \mathbb{R}^{n \times L}$ ($n < L$). The goal is to minimize the t -averaged mutual coherence $\mu_t(\mathbf{B}\Psi)$ with respect to \mathbf{B} . To compute $\mu_t(\mathbf{B}\Psi)$, the columns of $\mathbf{B}\Psi$ are normalized and then the Gram matrix $\mathbf{G} = (\mathbf{B}\Psi)^T(\mathbf{B}\Psi)$ is computed. The average of all entries $|\mathbf{G}_{ij}| \geq t$ is defined to be $\mu_t(\mathbf{B}\Psi)$. The proposed iterative solution algorithm proceeds in two alternating stages. Starting from some initial $\mathbf{B}^{(1)}$, in iteration i the Gram matrix $\mathbf{G}^{(i)} = (\mathbf{B}^{(i)}\Psi)^T(\mathbf{B}^{(i)}\Psi)$ is computed and its entries are modified such that $\mu_t(\mathbf{B}^{(i)}\Psi)$ decreases, yielding a new matrix $\hat{\mathbf{G}}^{(i)}$. In order to decrease $\mu_t(\mathbf{B}^{(i)}\Psi)$, a *down-scaling factor* $\gamma \in (0, 1)$, which is chosen before the algorithm's main iterations start, is used to *shrink* all entries of $\mathbf{G}^{(i)}$ whose absolute values are larger than t by multiplying them by γ . In the second stage, a decomposition $\hat{\mathbf{G}}^{(i)} \approx (\mathbf{B}^{(i+1)}\Psi)^T(\mathbf{B}^{(i+1)}\Psi)$ is found to obtain a new matrix $\mathbf{B}^{(i+1)}$. These two stages are alternated for a number of iterations.

Similar to [32], the authors of [33] work with the Gram matrix $\mathbf{G} \in \mathbb{R}^{L \times L}$. Their goal is to choose $\mathbf{B} \in \mathbb{R}^{m \times n}$

such that \mathbf{G} is as close to an identity matrix as possible. To this end, \mathbf{B} is initialized randomly and then a KSVD-like algorithm consisting of m (number of rows of \mathbf{B}) steps is computed. Additionally, an extension is proposed where also the dictionary Ψ can be optimized.

The goal of [34] is to choose \mathbf{B} such that a bi-Lipschitz condition is established. For given data points $\{\mathbf{h}_i\}_{i=1}^T$, this condition is expressed by replacing \mathbf{h} in (7) with differences $\mathbf{h}_i - \mathbf{h}_j$. Therefore, the authors first define the secant set $\mathcal{S} = \{ \frac{\mathbf{h}_i - \mathbf{h}_j}{\|\mathbf{h}_i - \mathbf{h}_j\|}, 1 \leq i < j \leq T \}$ and then express the bi-Lipschitz criterion for this set as $|||\mathbf{B}\mathbf{v}||^2 - 1| = |\mathbf{v}^T \mathbf{B}^T \mathbf{B} \mathbf{v} - 1| \leq \delta$ with $\mathbf{v} \in \mathcal{S}$. Using the Gram matrix $\mathbf{G} = \mathbf{B}^T \mathbf{B}$, this motivates the following optimization problem to find a matrix $\mathbf{B} \in \mathbb{R}^{m \times n}$:

$$\begin{aligned} \min_{\mathbf{G} \in \mathbb{R}^{n \times n}} \sup_{\mathbf{v} \in \mathcal{S}} |\mathbf{v}^T \mathbf{G} \mathbf{v} - 1| \\ \text{s.t. } \mathbf{G} \succeq 0, \quad \text{rank}(\mathbf{G}) = r, \quad \text{trace}(\mathbf{G}) = b. \end{aligned} \quad (24)$$

The solution algorithm is based on a relaxation of (24).

A related problem is studied in [35]:

$$\min_{\mathbf{G} \in \mathbb{R}^{n \times n}, \mathbf{G} = \mathbf{G}^T, \mathbf{G} \succeq 0} \text{trace}(\mathbf{G}) \quad \text{s.t. } \sup_{\mathbf{v} \in \mathcal{S}} |\mathbf{v}^T \mathbf{G} \mathbf{v} - 1| \leq \delta. \quad (25)$$

Once a feasible \mathbf{G}^* is determined, the matrix \mathbf{B} is found via an eigendecomposition of \mathbf{G}^* .

An approach motivated by neural network learning is presented in [36]. The signal model is $\mathbf{y} = \mathbf{B}\mathbf{s}$ with nonnegative sparse vectors $\mathbf{s} \in \mathbb{R}_+^n$ and $\mathbf{B} \in \mathbb{R}^{m \times n}$. Motivated by an ℓ_1 -norm minimization approach, the authors propose to utilize the following projected subgradient update rule to learn \mathbf{B} :

$$\mathbf{s}^{(i+1)} = \mathbf{s}^{(i)} - \frac{\beta}{i} (\mathbf{I} - \mathbf{B}^T \mathbf{B}) \text{sign}(\mathbf{s}^{(i)}) \quad (26)$$

with the initialization $\mathbf{s}^{(1)} = \mathbf{B}^T \mathbf{y}$ and $\beta \in \mathbb{R}$. Every gradient iteration (26) is interpreted as a layer and I such gradient layers are concatenated. This is called gradient unrolling. The final output and estimate for \mathbf{s} is given by $\hat{\mathbf{s}} = \text{ReLU}(\mathbf{s}^{(I+1)})$, where ReLU denotes the usual rectified linear unit which performs the operation $\max(x, 0)$ on every element x of its argument. Then, $\mathbf{B} \in \mathbb{R}^{m \times n}$ and $\beta \in \mathbb{R}$ are interpreted as learnable parameters and stochastic gradient descent is employed to learn \mathbf{B} and β . Specifically, given training data $\{\mathbf{s}_i\}_{i=1}^T$, a stochastic gradient descent method is used to solve

$$\min_{\mathbf{B} \in \mathbb{R}^{m \times n}, \beta \in \mathbb{R}} \frac{1}{T} \sum_{i=1}^T \|\mathbf{s}_i - \hat{\mathbf{s}}_i\|^2. \quad (27)$$

This gradient unrolling method was again employed in [37] for channel state information feedback. To this end, a channel $\mathbf{h} \in \mathbb{C}^n$ is compressed as $\mathbf{y} = \mathbf{B}[\Re(\mathbf{h})^T, \Im(\mathbf{h})^T]^T \in \mathbb{R}^m$ with $\mathbf{B} \in \mathbb{R}^{m \times 2n}$ such that the base station can recover \mathbf{h} from the feedback signal \mathbf{y} via compressive sensing methods. A modification of [36] for channel estimation is described in [38], where real and imaginary parts of channels $\mathbf{h} \in \mathbb{C}^n$ are treated as independent data points such that a real matrix $\mathbf{B} \in \mathbb{R}^{m \times n}$ can be learned.

Algorithm 3 LBCS [20]

Require: training data $\{\mathbf{h}_i\}_{i=1}^{T_{\text{tr}}}$
Require: matrix $\mathbf{V} \in \mathbb{C}^{n \times n}$, number m of rows to select

- 1: normalize the training data: $\{\tilde{\mathbf{h}}_i\}_{i=1}^{T_{\text{tr}}} \leftarrow \left\{ \frac{\mathbf{h}_i}{\|\mathbf{h}_i\|} \right\}_{i=1}^{T_{\text{tr}}}$
- 2: **for** $r = 1$ to n **do**
- 3: $\alpha_r \leftarrow \sum_{i=1}^{T_{\text{tr}}} |\langle \mathbf{v}_r, \tilde{\mathbf{h}}_i \rangle|^2$ (with \mathbf{v}_r row r of \mathbf{V})
- 4: **end for**
- 5: $\Omega \leftarrow$ indices r which correspond to m largest α_r
- 6: **return** $\mathbf{P}_\Omega \mathbf{V}$ (learned measurement matrix)

B. Learning-Based Compressive Subsampling (LBCS)

One challenge with the methods presented so far is that general real-valued matrices $\mathbf{B} \in \mathbb{R}^{m \times n}$ are found whereas we are seeking a complex-valued matrix $\mathbf{A} \in \mathbb{C}^{m \times n}$ where all entries $[\mathbf{A}]_{k,l}$ have the same absolute value. This constant modulus constraint is the main challenge. In particular, methods which are based on a decomposition of the form $\mathbf{G} = \mathbf{B}^T \mathbf{B}$ are difficult to apply since such a decomposition need not exist when the entries of \mathbf{B} are required to have a constant modulus. However, a modification of the approach published in [20] allows us to incorporate the constraint.

The approach investigated in [20] is based on the model

$$\mathbf{y} = \mathbf{P}_\Omega \mathbf{V} \mathbf{h} \quad (28)$$

where $\mathbf{V} \in \mathbb{C}^{n \times n}$ is a basis (a unitary matrix, $\mathbf{V}^H \mathbf{V} = \mathbf{I}$) and $\mathbf{P}_\Omega \in \mathbb{C}^{m \times n}$ performs subsampling by selecting $m = |\Omega|$ rows of \mathbf{V} . Once the row index set $\Omega \subset \{1, 2, \dots, n\}$ is chosen, the measurement matrix is given by $\mathbf{B} = \mathbf{P}_\Omega \mathbf{V} \in \mathbb{C}^{m \times n}$. One strategy is to select the indices Ω randomly. However, the authors of [20] argue that one can improve upon this by considering a data-based selection procedure.

A criterion for selecting Ω for which an exact solution is provided in [20] can be described as follows. Let $\{\mathbf{h}_i\}_{i=1}^T$ be given training data with norm one. Then, select those m rows $\mathbf{v}_r \in \mathbb{C}^n$ of \mathbf{V} which maximize $\frac{1}{T} \sum_{i=1}^T \sum_{r \in \Omega} |\langle \mathbf{v}_r, \mathbf{h}_i \rangle|^2$. This corresponds to maximizing the average captured energy $\|\mathbf{P}_\Omega \mathbf{V} \mathbf{h}_i\|^2$ of the observed data. We call the procedure LBCS after the paper's title and it is outlined in Algorithm 3.

C. Adaptation of LBCS

Since (28) considers the noiseless case and since it is assumed that a unitary matrix is already given, we suggest the following adaptation of the algorithm to obtain a matrix \mathbf{A} which can be employed in the context of the current paper.

Because we need a constant modulus matrix, the first modification is to divide the entries of \mathbf{V} by their respective absolute values. Algorithm 3 can then be used to select m rows of this constant modulus matrix. Second, we do a Monte Carlo search over different initializations of the unitary matrix \mathbf{V} . To explain, we draw a unitary matrix \mathbf{V} uniformly at random, divide its entries by their absolute values, and run Algorithm 3 to obtain a constant modulus matrix \mathbf{A} . An algorithm for generating random unitary matrices can, e.g., be found in [39]. Then, validation data $\{\mathbf{h}_i\}_{i=1}^{T_{\text{val}}}$ is used to evaluate the channel estimation performance of the current \mathbf{A}

Algorithm 4 Monte Carlo LBCS

Require: training and validation data $\{\mathbf{h}_j\}_{j=1}^{T_{\text{tr}}}$ and $\{\mathbf{h}_j\}_{j=1}^{T_{\text{val}}}$
Require: SNR, number m of rows to select, iterations I

- 1: $\mathbf{A}_{\text{MC}} \leftarrow \mathbf{0}$, $\text{MSE}_{\text{MC}} \leftarrow \infty$
- 2: **for** $i = 1$ to I **do**
- 3: draw a random unitary matrix $\mathbf{V} \in \mathbb{C}^{n \times n}$
- 4: divide all entries of \mathbf{V} by their absolute values
- 5: normalize the rows of \mathbf{V}
- 6: $\mathbf{A}^{(i)} \leftarrow \text{LBCS}(\{\mathbf{h}_j\}_{j=1}^{T_{\text{tr}}}, \mathbf{V}, m)$
- 7: $\text{MSE}^{(i)} \leftarrow \text{Evaluation}(\mathbf{A}^{(i)}, \{\mathbf{h}_j\}_{j=1}^{T_{\text{val}}}, \text{SNR})$
- 8: **if** $\text{MSE}^{(i)} < \text{MSE}_{\text{MC}}$ **then**
- 9: $\text{MSE}_{\text{MC}} \leftarrow \text{MSE}^{(i)}$
- 10: $\mathbf{A}_{\text{MC}} \leftarrow \mathbf{A}^{(i)}$
- 11: **end if**
- 12: **end for**
- 13: **return** \mathbf{A}_{MC}

in terms of mean squared error (MSE). The best matrix \mathbf{A}_{MC} of I such iterations is then the final result of the Monte Carlo search. The whole procedure is outlined in Algorithm 4.

D. Comparison between MMD-Based Learning and LBCS

Both Algorithm 2 and Algorithm 4 are data-based approaches to determine a matrix \mathbf{A} . In both cases, an outer loop over different initializations is used. Algorithm 2 would be combined with multiple random searches, and in case of Algorithm 4, we evaluate Algorithm 3 multiple times for different randomly initialized uniform matrices. These are the training phases of the respective algorithms. A main difference is that Algorithm 4 uses a validation MSE criterion to choose the best matrix, which is dependent on the SNR. Thus, in the numerical experiments in Section V, we run the algorithm for every SNR. This is in contrast to Algorithm 2 where a single matrix is determined which can be employed for all SNRs. Another difference is that Algorithm 4 selects rows of a random initialization \mathbf{V} , but doesn't modify its initial entries. In comparison, Algorithm 2 continually updates a random initialization.

V. NUMERICAL EXPERIMENTS

In numerical experiments, we cover the cases (i) training with sparse vectors, (ii) training with vectors that have an exact sparse representation, and (iii) training with vectors that are only approximately sparse. Channel estimation is always performed with OMP (Algorithm 1). While there are other choices for recovery algorithms, like ℓ_1 -norm minimization [14], the exact choice is not too critical since we are only interested in the relative performance of the different approaches to determine a measurement matrix. OMP is a cheap option and widely used.

A. Data Models

Of the following three data models, only the last would actually be considered a model for communications channels. Nonetheless, for simplicity, we continue to speak of channels

Algorithm 5 Evaluation

Require: measurement matrix \mathbf{A} , data $\{\mathbf{h}_i\}_{i=1}^T$
Require: SNR, sparsity p , dictionary Ψ

```

1:  $e \leftarrow 0, \Delta \leftarrow 0$ 
2: for  $i = 1$  to  $T$  do
3:   get  $\sigma$  with  $(\mathbf{A}, \mathbf{h}_i)$  via (3), draw  $\mathbf{n} \sim \mathcal{CN}(\mathbf{0}_m, \sigma^2 \mathbf{I}_m)$ 
4:    $\mathbf{y} \leftarrow \mathbf{A}\mathbf{h}_i + \mathbf{n}$  (compute observation)
5:    $\hat{\mathbf{h}} \leftarrow \Psi\text{OMP}(\mathbf{A}\Psi, \mathbf{y}, p)$  (estimate channel  $\mathbf{h}_i$ )
6:    $e \leftarrow e + \|\mathbf{h}_i\|^2, \Delta \leftarrow \Delta + \|\hat{\mathbf{h}} - \mathbf{h}_i\|^2$  (squared error)
7: end for
8: return  $\frac{\Delta}{e}$  (relative mean squared error)
```

and channel estimation. We investigate these three models because they represent typical cases of CS applications.

First, channels

$$\mathbf{h} = \mathbf{s} \quad (29)$$

are modeled as sparse vectors $\mathbf{s} \in \mathbb{C}^n$ with p nonzero entries. Second, channels are modeled as sparse with respect to the discrete Fourier transform (DFT) basis $\mathbf{F} \in \mathbb{C}^{n \times n}$:

$$\mathbf{h} = \mathbf{F}\mathbf{s}. \quad (30)$$

In both cases, each of the p nonzero entries of \mathbf{s} is drawn from a Gaussian distribution $\mathcal{CN}(0, \frac{1}{p})$. Third, channels are modeled as explained around (4) such that we have

$$\mathbf{h} = \sum_{k=1}^p s_k \mathbf{a}(\theta_k). \quad (31)$$

The path gains s_k are drawn from $\mathcal{CN}(0, \frac{1}{p})$, the angles θ_k are drawn uniformly in $[0, 2\pi]$. To perform channel estimation, we use the dictionary Ψ_L from (8) with $L = 16n$.

To estimate a channel \mathbf{h} from an observation $\mathbf{y} = \mathbf{A}\mathbf{h} + \mathbf{n}$, OMP (Algorithm 1) is used with $\mathbf{C} = \mathbf{A}\Psi$ where Ψ is chosen as (i) $\Psi = \mathbf{I}$, (ii) $\Psi = \mathbf{F}$, or (iii) $\Psi = \Psi_L$, depending on the channel model. In all cases, OMP yields a p -sparse vector $\hat{\mathbf{s}}$ and the channel estimate is computed as $\hat{\mathbf{h}} = \Psi\hat{\mathbf{s}}$. In the following numerical experiments, the described procedure is repeated for $T_{\text{test}} = 10000$ randomly drawn channels such that an overall relative MSE $\frac{\mathbb{E}[\|\hat{\mathbf{h}} - \mathbf{h}\|^2]}{\mathbb{E}[\|\mathbf{h}\|^2]}$ can be estimated. For a given measurement matrix \mathbf{A} determined via learning (Algorithm 2) or via LBCS (Algorithm 4), the evaluation process is outlined in Algorithm 5.

As already pointed out in Section IV, the related methods which are based on decompositions of a Gram matrix are difficult to employ when the measurement matrix is constrained to have constant modulus entries because a corresponding decomposition does generally not exist. However, the method from [20] could be adapted to the constraint and is therefore used as a reference, see Algorithm 4.

We compare the two methods of determining a measurement matrix \mathbf{A} (Algorithms 2 and 4) with the alternative approach of drawing a new random measurement matrix for every channel. That is, instead of first fixing \mathbf{A} and then running Algorithm 5, the first step in the for-loop (between lines 2 and 3) always consists of drawing a new random measurement matrix (with entries as explained in (10)) such that as many measurement

matrices are drawn as there are channels. This approach is labeled as “random” in the following plots.

B. Implementation Details

Whenever we run Algorithm 4, we use $T_{\text{tr}} = 100000$ training and $T_{\text{val}} = 1000$ validation data samples which are randomly generated according to one of the three channel models. Further, for every given SNR, we do a Monte Carlo search over $I = 100$ matrices.

In order to run the learning Algorithm 2, a number of hyperparameters need to be set. First of all, since we use MMD with a Gaussian kernel (15), the parameter $\sigma > 0$ needs to be chosen. As argued in [17], finding the optimal σ which makes MMD most efficient is an open problem, but a mixture of kernels may serve the intended purpose. Therefore, we use MMD_k in (17) with the kernel

$$k(x, y) = \sum_{\sigma \in \mathcal{S}} k_{\sigma}(x, y) \quad (32)$$

where $\mathcal{S} = \{2, 5, 10, 20, 40, 80\}$.

We use Pytorch [40] to implement the stochastic gradient optimization in Algorithm 2 with the Adam optimizer [41]. There are three hyperparameters: batch size T , learning rate (gradient step size) l_r , and exponential learning rate decay β . As described in [42], we determine these three hyperparameters via random search. In detail, we draw $(T, l_r, \beta) \in [150, 1500] \times [10^{-6}, 5 \cdot 10^{-3}] \times [0.94, 1]$ randomly and run Algorithm 2. This is repeated 64 times and validation data is then used to pick the best of the 64 so-obtained matrices \mathbf{A} . The number of training samples is always $T_{\text{tr}} = 50000$ in all cases and settings. For reasons explained later in Section V-E, training data points $\{\mathbf{h}_i\}_{i=1}^{T_{\text{tr}}}$ are normalized as follows:

$$\tilde{\mathbf{h}}_i = \frac{\mathbf{h}_i}{\sqrt{\frac{1}{T_{\text{tr}}} \sum_{j=1}^{T_{\text{tr}}} \|\mathbf{h}_j\|^2}}, \quad \forall i = 1, 2, \dots, T_{\text{tr}}. \quad (33)$$

The termination criterion for Algorithm 2 is early stopping [43].

C. Discussion of Results for Sparse Vectors

We first concentrate on the two models (29) and (30) where channels have an exact sparse representation (either in the canonical basis \mathbf{I} or in the DFT basis \mathbf{F}). The constant modulus measurement matrix $\mathbf{A} \in \mathbb{C}^{m \times 128}$ has the dimensions $m \times 128$ and we vary the sparsity $p \in \{1, 5, 10\}$.

The left plot in Fig. 1 visualizes evaluation results with model (29) for $m = 16$. Generally, we can see that recovering channels with sparsity $p = 10$ from $m = 16$ measurements is not possible: the relative MSE is larger than one. The case $p = 5$ shows better performance and the case $p = 1$ seems to show perfect recovery up to the remaining error which is due to noise. Given the fact that we try to recover p nonzero entries of an $n = 128$ -dimensional sparse vector from only $m = 16$ measurements, the qualitative behavior of the displayed curves can be expected.

It is worth pointing out that while the performance of the three displayed methods of generating measurement matrices

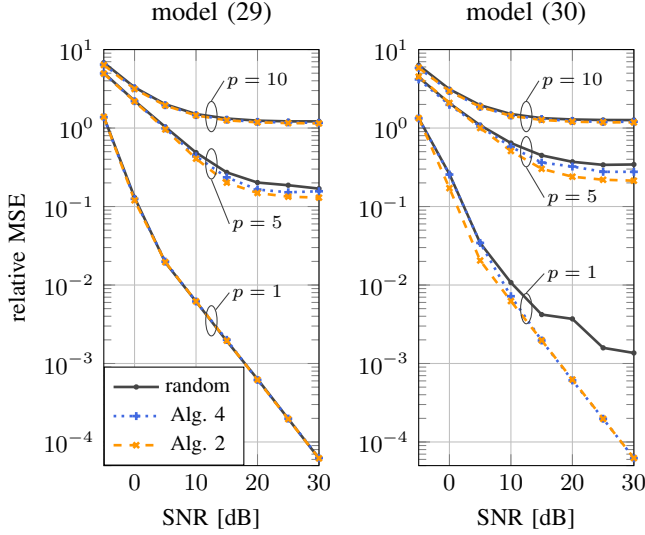


Fig. 1. Evaluation with channel models (29) (left) and (30) (right). The constant modulus matrices \mathbf{A} have size 16×128 and the sparsity $p \in \{1, 5, 10\}$ is varied. Evaluation is shown with random matrices (—), with the matrices from Algorithm 4 (····), and with the matrices from Algorithm 2 (---).

is aligned in the case $p = 1$, we only have one matrix per SNR when Algorithm 4 is used and we only have a single matrix for the whole curve when the proposed Algorithm 2 is used. In contrast, the random matrices approach generates a new random matrix for every channel. All three methods lead to equally bad performance for $p = 10$ where the limiting factor seems to be the too small number of measurements $m = 16$. Further, for $p = 5$, both Algorithms 2 and 4 improve on random matrices.

The right plot in Fig. 1 visualizes the same setting but with model (30). According to compressive sensing theory, there should not be a performance difference between the two channel models (29) or (30) when random matrices are employed. This is due to the fact that random matrices enjoy a universality property which means that they are incoherent to any basis [14]. However, the case $p = 1$ in the right plot clearly behaves differently from the corresponding case in the left plot. We can understand this behavior when we take into account that both the random constant modulus matrices \mathbf{A} as well as the DFT basis \mathbf{F} have entries of the form $e^{j\phi}$. This can lead to a large coherence between \mathbf{A} and \mathbf{F} which can degrade the performance. Remarkably, Algorithms 2 and 4 show equally good performance in both cases: the respective training processes are able to find incoherent enough measurement matrices. Even in the simple case $p = 1$, the observed behavior of the algorithms is already interesting. It emphasizes the difference in the obtained matrices.

Fig. 2 repeats the experiments for $m = 32$. It can be seen that now all cases $p \in \{1, 5, 10\}$ show a relative MSE below one which can be interpreted to mean that the number of measurements m starts to be large enough. Additionally, we observe that the case $p = 5$ starts to be parallel to $p = 1$ which is to be expected once m is large enough. Further, the incoherence problem for model (30) in contrast to model (29) is not as pronounced anymore which further supports the

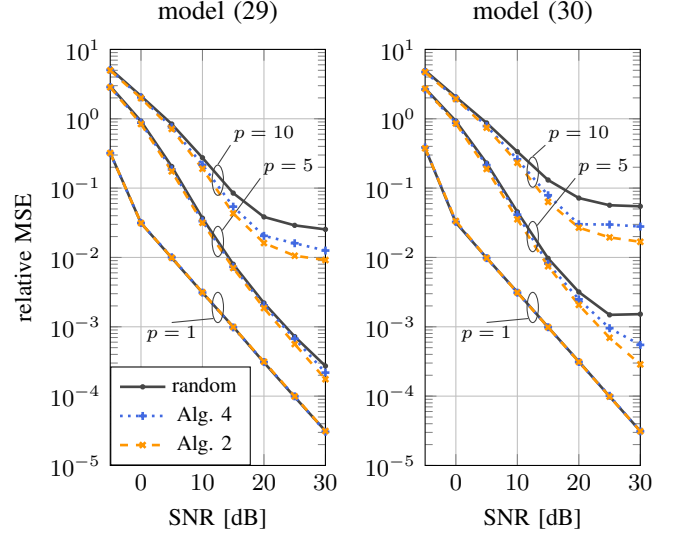


Fig. 2. Evaluation with channel models (29) (left) and (30) (right). The constant modulus matrices \mathbf{A} have size 32×128 and the sparsity $p \in \{1, 5, 10\}$ is varied. Evaluation is shown with random matrices (—), with the matrices from Algorithm 4 (····), and with the matrices from Algorithm 2 (---).

provided explanation. Still, a degradation can be observed in the right plot for $p = 5$ and again Algorithms 2 and 4 can alleviate the problem. Lastly, we see how the two learning-based methods improve on random matrices in particular for $p = 10$.

We also simulated $m = 64$ and $m = 96$ where all curves essentially are straight lines and all methods are aligned (not shown here). At this point, we would like to emphasize again that this is a satisfying result since, e.g., the proposed Algorithm 2 gives us a single measurement matrix that we use for all SNRs, which may offer attractive options for potential technical implementations.

D. Discussion of Results for Approximately Sparse Vectors

This subsection concentrates on channel model (31). Fig. 3 shows the evaluation of matrices $\mathbf{A} \in \mathbb{C}^{m \times 128}$ with $m \in \{32, 64, 96\}$ for $p = 5$ (left) and $p = 10$ (right) paths. We see that all curves are eventually constant with increasing SNR. The reason for this phenomenon is that the channels are only approximately sparse: $\mathbf{h} \approx \Psi_L \mathbf{s}$. Thus, even in the noiseless case, perfect recovery is not possible whenever angles θ_k of some steering vectors lie in between two grid points of the dictionary Ψ_L . There exist different approaches to combat this problem. On overview of grid-less methods can, e.g., be found in [44, Chapter 11]. However, since we are only interested in studying the behavior of different measurement matrices rather than in the actual channel estimation itself, it suffices for our purposes to work with the on-grid OMP algorithm.

In all cases, Algorithms 2 and 4 can significantly improve on random matrices. Consider for example the cases $m \in \{64, 96\}$ in the left plot of Fig. 3. The performance of the matrices for $m = 64$ of Algorithms 2 and 4 reaches the performance of random matrices for $m = 96$. In this sense, the learning processes lead to an improvement of the matrix \mathbf{A}

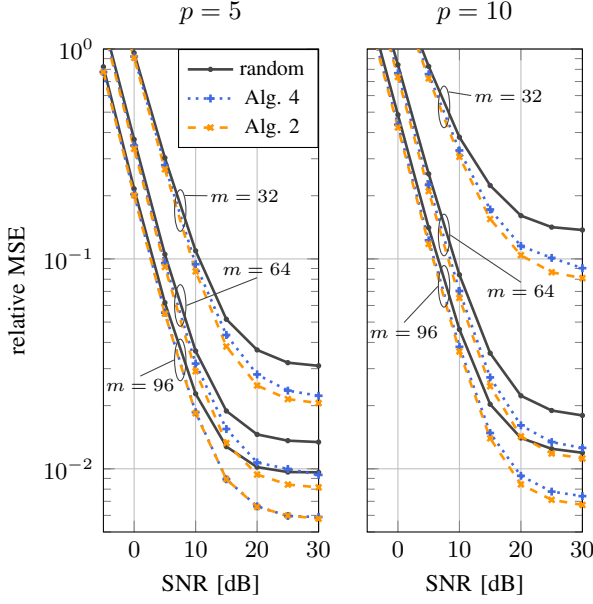


Fig. 3. Evaluation with channel model (31). The constant modulus matrices \mathbf{A} have size $m \times 128$ where $m \in \{32, 64, 96\}$. The number of paths is $p = 5$ (left) and $p = 10$ (right). Evaluation is shown with random matrices (\longrightarrow), with the matrices from Algorithm 4 ($\cdots\cdots$) and from Algorithm 2 ($\cdots\cdots$).

which corresponds to a gain of 32 measurements. Additionally, it can be kept in mind that Algorithms 2 and 4 only need one matrix (per SNR in case of Algorithm 4) in contrast to the random matrices approach.

We see a considerable performance degradation for the case $m = 32$ when p is increased from 5 to 10 (compare left and right plots in Fig. 3). This may again be interpreted as having a too small number of measurements m .

So far, in all considered cases, Algorithms 2 and 4 were at least as good or better than random matrices and the proposed Algorithm 2 was at least as good or better than Algorithm 4. However, this changes if we consider $m = 96$ and $p = 1$, which is displayed in Fig. 4. In theory, every matrix which can be found via Algorithm 4 is a matrix which could also be found via Algorithm 2, so that we could expect the performance of Algorithm 2 to be comparable to the one of Algorithm 4. In addition to the discussed hyperparameters, which we determine via random search, another important factor of Algorithm 2 is the initialization of the matrix Φ . In all considered numerical results, for initialization, every element was drawn independently and uniformly in the interval $[0, 2\pi]$. It is now an interesting experiment to initialize Algorithm 2 with Algorithm 4 and to observe whether the learning procedure does at least not degrade the quality of the final matrix.

This was done in Fig. 4 where we used Algorithm 4 with $\text{SNR} = 20$ dB to initialize Algorithm 2 before we run the 64 random searches as described in Section V-B. The corresponding curve reveals that the two algorithms harmonize well. Finding a good initialization is a general issue of gradient descent algorithms. The observation in Fig. 4 suggests to make initialization via Algorithm 4 part of the random search: in one half of all cases, the initialization would be random, in the

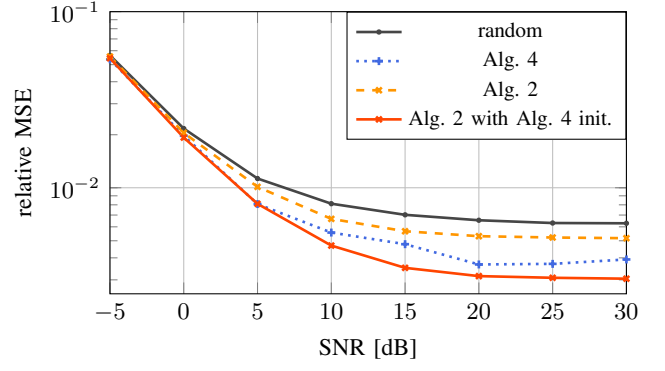


Fig. 4. Evaluation with channel model (31). The constant modulus matrices \mathbf{A} have size 96×128 . The number of paths is $p = 1$. Evaluation is shown with random matrices (\longrightarrow), and with the matrices from Algorithm 4 ($\cdots\cdots$) and from Algorithm 2 ($\cdots\cdots$). Further, the result of initializing Algorithm 2 with Algorithm 4 is depicted (\longrightarrow).

other half, the initialization would be based on Algorithm 4.

E. Training Data Normalization

Lastly, we want to discuss training data preprocessing for Algorithm 2. The initial idea described in Section III is to regard $\mathbf{A} \in \mathbb{C}^{m \times n}$ as a mapping from one hypersphere (in \mathbb{C}^n) to another hypersphere (in \mathbb{C}^m). This implies to normalize the training data $\{\mathbf{h}_i\}_{i=1}^{T_{\text{tr}}}$ via

$$\tilde{\mathbf{h}}_i = \frac{\mathbf{h}_i}{\|\mathbf{h}_i\|}, \quad \forall i = 1, 2, \dots, T_{\text{tr}} \quad (34)$$

such that $\tilde{\mathbf{h}}_i$ represents a point on the hypersphere in \mathbb{C}^n .

However, if the distribution of $\mathbf{A}\tilde{\mathbf{h}}$ now equaled the distribution of \mathbf{u} (cf. (13)), we would have $\|\mathbf{A}\tilde{\mathbf{h}}\| = 1$ which means we would have found a matrix with RIP constant δ equal to zero, see (11). This can be expected to be difficult if not impossible. In particular, if the number of rows, m , is significantly smaller than the number of columns, n , then δ can be expected to be relatively large. On the other hand, if m is larger, the matrix \mathbf{A} is closer to a square matrix and it is easier to find an (approximate) isometry. With this intuition in mind, the optimization problem may be difficult to solve if the data is normalized such that every $\tilde{\mathbf{h}}_i$ lies exactly on the hypersphere in \mathbb{C}^n , i.e., if we have $\|\tilde{\mathbf{h}}_i\| = 1$. To alleviate the problem, we heuristically introduce some variation in the norm of the training data. Specifically, we normalize the training data as described in equation (33), where the denominator approximates $\sqrt{\mathbb{E}[\|\mathbf{h}\|^2]}$. Consequently, the training data points are only “on average” on the hypersphere in \mathbb{C}^n . Now, the distribution $\mathbf{A}\tilde{\mathbf{h}}$ can be equal to the distribution of \mathbf{u} , but we would not have $\delta = 0$.

The effect of the different normalizations is studied in Fig. 5 where we consider two extreme cases: few measurements $m = 16$ but only a single path $p = 1$ and many measurements $m = 96$ with many paths $p = 10$. It can be seen that the normalization (33) leads to better results than (34). The difference is particularly pronounced in the case $m = 16$. This fits the intuition provided above: as m decreases, δ potentially needs to increase. Hence, training with (34) is more restrictive

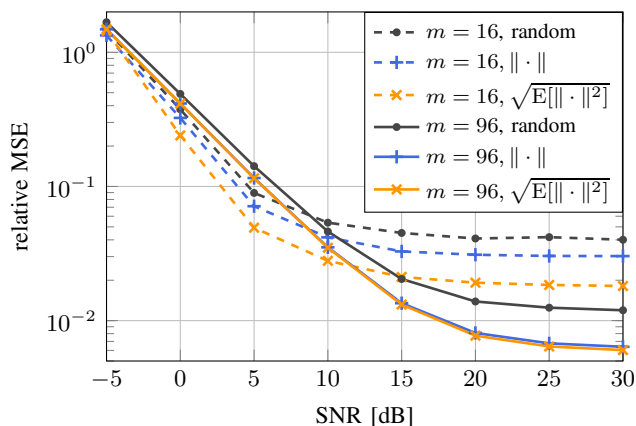


Fig. 5. Dashed curves show evaluation with model (31) for $m = 16$ and $p = 1$, solid curves for $m = 96$ and $p = 10$. Evaluation with random constant modulus matrices is displayed in dark gray ($- \bullet -$, $- \bullet -$). Blue curves ($- + -$, $- + -$) refer to learning a matrix with training data normalization $\mathbf{h}/\|\mathbf{h}\|$, orange curves ($- \times -$, $- \times -$) refer to normalization $\mathbf{h}/\sqrt{E[\|\mathbf{h}\|^2]}$.

in that case. Motivated by Fig. 5, normalization (33) was used in all other numerical experiments presented in this section.

VI. CONCLUSION

The anchor point of our studies was the interpretation that a measurement matrix which has the RIP constitutes (approximately) a mapping between hyperspheres. In order to take measurement noise into account, we proposed to determine the measurement matrix such that it maps points uniformly onto the hypersphere in its range. One of the MMD metrics was used to measure the distance between a uniform distribution on the hypersphere and the distribution in the range of the measurement matrix. The recent success of MMD-based machine learning applications motivated a solution of the optimization problem via stochastic gradient descent. Further, it was shown that a modified method from the literature also leads to good performance and that it can harmonize with our approach by providing a suitable initialization for the learning algorithm.

The algorithm's learning phase requires training data. This training data may, for example, be obtained by means of a measurement campaign. The learned matrix will then depend on the measured scenario. In our experiments, this is reflected by the matrix's dependency on the number of propagation paths. In this context, it might be interesting to investigate how the performance behaves when the scenario changes. One might then attempt to employ a form of domain adaptation [43] to adaptively update the measurement matrix.

A notable property of the proposed learning algorithm is that it yields one measurement matrix which can be employed for all SNRs. Numerical experiments demonstrate this property and the great performance of the proposed method.

In this paper, we focused on measurement matrices with a constant modulus constraint. We translated the constraint into the system of equations shown in (21). For an arbitrary (not

necessarily constant modulus) matrix $\mathbf{C} \in \mathbb{C}^{m \times n}$, (21) takes the form

$$\begin{bmatrix} \Re(\mathbf{C}\tilde{\mathbf{h}}) \\ \Im(\mathbf{C}\tilde{\mathbf{h}}) \end{bmatrix} = \begin{bmatrix} \Re(\mathbf{C}) & -\Im(\mathbf{C}) \\ \Im(\mathbf{C}) & \Re(\mathbf{C}) \end{bmatrix} \begin{bmatrix} \Re(\tilde{\mathbf{h}}) \\ \Im(\tilde{\mathbf{h}}) \end{bmatrix}. \quad (35)$$

It can be seen that more general structural constraints can be incorporated into the design of \mathbf{C} as well. For example, the authors of [45] prove that random Toeplitz matrices can satisfy a RIP condition and use this result to motivate the application of such matrices in a channel estimation context. A Toeplitz measurement matrix can also be learned with the approach described in Section III-B. To this end, weight tying can be employed [43]. That is, parameters of \mathbf{C} would be shared between rows to enforce a Toeplitz structure. Here it makes sense to normalize the rows during training. Similarly, other structured matrices can be learned too.

REFERENCES

- [1] Z. Pi and F. Khan, "An introduction to millimeter-wave mobile broadband systems," *IEEE Commun. Mag.*, vol. 49, no. 6, pp. 101–107, Jun. 2011.
- [2] T. S. Rappaport, S. Sun, R. Mayzus, H. Zhao, Y. Azar, K. Wang, G. N. Wong, J. K. Schulz, M. Samimi, and F. Gutierrez, "Millimeter wave mobile communications for 5G cellular: It will work!" *IEEE Access*, vol. 1, pp. 335–349, 2013.
- [3] S. Sun, T. S. Rappaport, R. W. Heath, A. Nix, and S. Rangan, "MIMO for millimeter-wave wireless communications: Beamforming, spatial multiplexing, or both?" *IEEE Commun. Mag.*, vol. 52, no. 12, pp. 110–121, Dec. 2014.
- [4] T. Bai, A. Alkhateeb, and R. W. Heath, "Coverage and capacity of millimeter-wave cellular networks," *IEEE Commun. Mag.*, vol. 52, no. 9, pp. 70–77, Sep. 2014.
- [5] F. Boccardi, R. W. Heath, A. Lozano, T. L. Marzetta, and P. Popovski, "Five disruptive technology directions for 5G," *IEEE Commun. Mag.*, vol. 52, no. 2, pp. 74–80, Feb. 2014.
- [6] O. E. Ayach, S. Rajagopal, S. Abu-Surra, Z. Pi, and R. W. Heath, "Spatially sparse precoding in millimeter wave MIMO systems," *IEEE Trans. Wireless Commun.*, vol. 13, no. 3, pp. 1499–1513, Mar. 2014.
- [7] L. Liang, W. Xu, and X. Dong, "Low-complexity hybrid precoding in massive multiuser MIMO systems," *IEEE Wireless Commun. Lett.*, vol. 3, no. 6, pp. 653–656, Dec. 2014.
- [8] A. Alkhateeb, O. El Ayach, G. Leus, and R. W. Heath, "Channel estimation and hybrid precoding for millimeter wave cellular systems," *IEEE J. Sel. Topics Signal Process.*, vol. 8, no. 5, pp. 831–846, Oct. 2014.
- [9] R. Méndez-Rial, C. Rusu, N. González-Prelcic, A. Alkhateeb, and R. W. Heath, "Hybrid mimo architectures for millimeter wave communications: Phase shifters or switches?" *IEEE Access*, vol. 4, pp. 247–267, 2016.
- [10] K. Ardah, G. Fodor, Y. C. B. Silva, W. C. Freitas, and F. R. P. Cavalcanti, "A unifying design of hybrid beamforming architectures employing phase shifters or switches," *IEEE Trans. Veh. Technol.*, vol. 67, no. 11, pp. 11 243–11 247, Nov. 2018.
- [11] W. U. Bajwa, J. Haupt, A. M. Sayeed, and R. Nowak, "Compressed channel sensing: A new approach to estimating sparse multipath channels," *Proc. IEEE*, vol. 98, no. 6, pp. 1058–1076, Jun. 2010.
- [12] A. Alkhateeb, G. Leus, and R. W. Heath, "Compressed sensing based multi-user millimeter wave systems: How many measurements are needed?" in *2015 IEEE Int. Conf. Acoustics, Speech and Signal Process. (ICASSP)*, 2015, pp. 2909–2913.
- [13] T. Kim and D. J. Love, "Virtual AoA and AoD estimation for sparse millimeter wave MIMO channels," *2015 IEEE 16th Int. Workshop Signal Process. Advances in Wireless Commun. (SPAWC)*, pp. 146–150, 2015.
- [14] S. Foucart and H. Rauhut, *A Mathematical Introduction to Compressive Sensing*. Birkhäuser Basel, 2013.
- [15] V. Venkateswaran and A.-J. van der Veen, "Analog beamforming in MIMO communications with phase shift networks and online channel estimation," *IEEE Trans. Signal Process.*, vol. 58, no. 8, pp. 4131–4143, Aug. 2010.
- [16] A. Gretton, K. M. Borgwardt, M. J. Rasch, B. Schölkopf, and A. Smola, "A kernel two-sample test," *J. Mach. Learn. Res.*, vol. 13, no. 1, pp. 723–773, Mar. 2012.

- [17] Y. Li, K. Swersky, and R. Zemel, "Generative moment matching networks," in *Proc. 32nd Int. Conf. on Mach. Learn. - Volume 37*, ser. ICML'15. JMLR.org, 2015, p. 1718–1727.
- [18] C.-L. Li, W.-C. Chang, Y. Cheng, Y. Yang, and B. Poczos, "MMD GAN: Towards deeper understanding of moment matching network," in *Advances in Neural Inf. Process. Systems 30*, I. Guyon, U. V. Luxburg, S. Bengio, H. Wallach, R. Fergus, S. Vishwanathan, and R. Garnett, Eds. Curran Associates, Inc., 2017, pp. 2203–2213.
- [19] G. K. Dziugaite, D. M. Roy, and Z. Ghahramani, "Training generative neural networks via maximum mean discrepancy optimization," in *Proc. 31st Conf. on Uncertainty in Artificial Intelligence*, ser. UAI'15. Arlington, Virginia, USA: AUAI Press, 2015, p. 258–267.
- [20] L. Baldassarre, Y. Li, J. Scarlett, B. Gözçü, I. Bogunovic, and V. Cevher, "Learning-based compressive subsampling," *IEEE J. Sel. Topics Signal Process.*, vol. 10, no. 4, pp. 809–822, Jun. 2016.
- [21] Y. C. Eldar and M. Mishali, "Robust recovery of signals from a structured union of subspaces," *IEEE Trans. Inf. Theory*, vol. 55, no. 11, pp. 5302–5316, Nov. 2009.
- [22] T. Blumensath, "Sampling and reconstructing signals from a union of linear subspaces," *IEEE Trans. Inf. Theory*, vol. 57, no. 7, pp. 4660–4671, Jul. 2011.
- [23] T. Wiese, L. Weiland, and W. Utschick, "Inexact projected gradients on unions of subspaces," in *2017 IEEE Int. Symp. Inf. Theory (ISIT)*, 2017, pp. 236–240.
- [24] G. Davis, S. Mallat, and M. Avellaneda, "Adaptive greedy approximations," *Constructive Approximation*, vol. 13, no. 1, pp. 57–98, Mar. 1997.
- [25] Y. C. Pati, R. Rezaeiifar, and P. S. Krishnaprasad, "Orthogonal matching pursuit: Recursive function approximation with applications to wavelet decomposition," in *Proc. 27th Asilomar Conf. Signals, Systems and Computers*, Nov. 1993, pp. 40–44 vol.1, ISSN: 1058-6393.
- [26] J. A. Tropp, "Greed is good: Algorithmic results for sparse approximation," *IEEE Trans. Inf. Theory*, vol. 50, no. 10, pp. 2231–2242, Oct. 2004.
- [27] B. K. Sriperumbudur, A. Gretton, K. Fukumizu, B. Schölkopf, and G. R. Lanckriet, "Hilbert space embeddings and metrics on probability measures," *J. Mach. Learn. Res.*, vol. 11, pp. 1517–1561, Aug. 2010.
- [28] Y. Ren, J. Li, Y. Luo, and J. Zhu, "Conditional generative moment-matching networks," in *Advances in Neural Information Processing Systems 29*, D. D. Lee, M. Sugiyama, U. V. Luxburg, I. Guyon, and R. Garnett, Eds. Curran Associates, Inc., 2016, pp. 2928–2936.
- [29] H. Gao and H. Huang, "Joint generative moment-matching network for learning structural latent code," in *Proceedings of the Twenty-Seventh International Joint Conference on Artificial Intelligence, IJCAI-18*. International Joint Conferences on Artificial Intelligence Organization, 7 2018, pp. 2121–2127.
- [30] A. Griewank and A. Walther, *Evaluating Derivatives: Principles and Techniques of Algorithmic Differentiation*, 2nd ed. USA: Society for Industrial and Applied Mathematics, 2008.
- [31] Y. Weiss, H. S. Chang, and W. T. Freeman, "Learning compressed sensing," in *Proc. Allerton Conf. Communication, Control and Computing*, 2007.
- [32] M. Elad, "Optimized projections for compressed sensing," *IEEE Trans. Signal Process.*, vol. 55, no. 12, pp. 5695–5702, Dec. 2007.
- [33] J. M. Duarte-Carvajalino and G. Sapiro, "Learning to sense sparse signals: Simultaneous sensing matrix and sparsifying dictionary optimization," *IEEE Trans. Image Process.*, vol. 18, no. 7, pp. 1395–1408, Jul. 2009.
- [34] A. Sadeghian, B. Bah, and V. Cevher, "Energy-aware adaptive bi-Lipschitz embeddings," in *Proc. 10th Int. Conf. Sampling Theory and Applications*, 07 2013.
- [35] C. Hegde, A. C. Sankaranarayanan, W. Yin, and R. G. Baraniuk, "NuMax: A convex approach for learning near-isometric linear embeddings," *IEEE Trans. Signal Process.*, vol. 63, no. 22, pp. 6109–6121, Nov. 2015.
- [36] S. Wu, A. Dimakis, S. Sanghavi, F. Yu, D. Holtmann-Rice, D. Storchus, A. Rostamizadeh, and S. Kumar, "Learning a compressed sensing measurement matrix via gradient unrolling," in *Proc. 36th Int. Conf. Mach. Learn.*, ser. Proceedings of Machine Learning Research, K. Chaudhuri and R. Salakhutdinov, Eds., vol. 97. PMLR, Jun. 2019, pp. 6828–6839.
- [37] P. Wu, Z. Liu, and J. Cheng, "Compressed CSI feedback with learned measurement matrix for mmWave massive MIMO," *arXiv e-prints*, p. arXiv:1903.02127, Mar. 2019.
- [38] P. Wu and J. Cheng, "Acquiring measurement matrices via deep basis pursuit for sparse channel estimation in mmWave massive MIMO systems," *arXiv e-prints*, p. arXiv:2007.05177, Jul. 2020.
- [39] F. Mezzadri, "How to generate random matrices from the classical compact groups," *Notices of the American Mathematical Society*, vol. 54, Oct. 2006.
- [40] A. Paszke, S. Gross, F. Massa, A. Lerer, J. Bradbury, G. Chanan, T. Killeen, Z. Lin, N. Gimeshine, L. Antiga, A. Desmaison, A. Kopf, E. Yang, Z. DeVito, M. Raison, A. Tejani, S. Chilamkurthy, B. Steiner, L. Fang, J. Bai, and S. Chintala, "Pytorch: An imperative style, high-performance deep learning library," in *Advances in Neural Inf. Process. Systems*, vol. 32. Curran Associates, Inc., 2019, pp. 8026–8037.
- [41] D. P. Kingma and J. Ba, "Adam: A method for stochastic optimization," in *Proc. 3rd Int. Conf. Learn. Representations, ICLR 2015*, Y. Bengio and Y. LeCun, Eds., 2015.
- [42] J. Bergstra and Y. Bengio, "Random search for hyper-parameter optimization," *J. Mach. Learn. Res.*, vol. 13, no. null, p. 281–305, Feb. 2012.
- [43] I. Goodfellow, Y. Bengio, and A. Courville, *Deep Learning*. MIT Press, 2016, <http://www.deeplearningbook.org>.
- [44] Z. Yang, J. Li, P. Stoica, and L. Xie, "Sparse methods for direction-of-arrival estimation," in *Academic Press Library in Signal Process., Volume 7*, 2018, pp. 509–581.
- [45] J. Haupt, W. U. Bajwa, G. Raz, and R. Nowak, "Toeplitz compressed sensing matrices with applications to sparse channel estimation," *IEEE Trans. Inf. Theory*, vol. 56, no. 11, pp. 5862–5875, Nov. 2010.